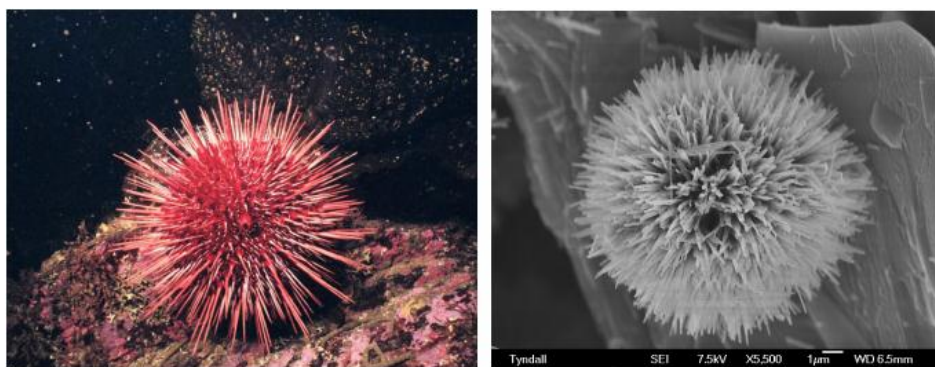


Title	Nano-urchin: The formation and structure of high-density spherical clusters of vanadium oxide nanotubes
Authors	O'Dwyer, Colm;Navas, D.;Lavayen, Vladimir;Benavente, Eglantina;Santa-Ana, María A.;Gonzalez, Guillermo;Newcomb, Simon B.;Sotomayor Torres, Clivia M.
Publication date	2006-01
Original Citation	O'Dwyer, C,Navas, D,Lavayen, V,Benavente, E,Santa Ana, MA,Gonzalez, G,Newcomb, SB,Torres, CMS (2006) 'Nano-urchin: The formation and structure of high-density spherical clusters of vanadium oxide nanotubes'. Chemistry of Materials, 18 (13), pp. 3016-3022. doi: 10.1021/cm0603809
Type of publication	Article (peer-reviewed)
Link to publisher's version	http://pubs.acs.org/doi/abs/10.1021/cm0603809 - 10.1021/cm0603809
Rights	© 2006, American Chemical Society. This document is the Accepted Manuscript version of a Published Work that appeared in final form in Chemistry of Materials, copyright © American Chemical Society after peer review and technical editing by the publisher.To access the final edited and published work see http://pubs.acs.org/doi/abs/10.1021/cm0603809
Download date	2024-04-27 14:33:41
Item downloaded from	https://hdl.handle.net/10468/987



UCC

University College Cork, Ireland
 Coláiste na hOllscoile Corcaigh



Sea Urchin

'NanoUrchin'

Manuscript Title: NanoUrchin: The Formation and Structure of High Density Spherical Clusters of Vanadium Oxide Nanotubes

Authors: C. O'Dwyer, D. Navas, V. Lavayen, E. Benavente, M. A. Santa Ana, G. González, S. B. Newcomb, and C. M. Sotomayor Torres

Urchin-like nanostructures consisting of high-density spherical nanotube radial arrays of VO_x nanocomposite. They form in stages, starting with radial arrangement of lamina followed by rolling into VO_x nanotubes with a density of $\sim 40 \text{ sr}^{-1}$. The nanotubes are several micrometers in length with inner hollow diameters of $\sim 75 \text{ nm}$.

NanoUrchin: The Formation and Structure of High Density Spherical Clusters of Vanadium Oxide Nanotubes

C. O'Dwyer,[†] D. Navas,[‡] V. Lavayen,^{*,†} E. Benavente,[‡] M. A. Santa Ana,^a G. González,^a
S. B. Newcomb,^b and C. M. Sotomayor Torres[†]

[†] *Tyndall National Institute, University College Cork, Lee Maltings, Cork, Ireland*

[‡] *Department of Chemistry, Universidad Tecnológica Metropolitana, Av. Jose Pedro
Alessandri, Santiago, Chile*

^a *Department of Chemistry, Faculty of Science, Universidad de Chile, P.O. Box 653,
Santiago, Chile*

^b *Glebe Scientific Ltd., Newport, Co. Tipperary, Ireland*

Keywords: Nanotube, nanocomposite, nanostructure, self-assembly, vanadium oxide

Abstract

We report the observation of urchin-like nanostructures consisting of high-density spherical nanotube radial arrays of vanadium oxide nanocomposite, successfully synthesized by a simple chemical route using an ethanolic solution of vanadium tri-isopropoxide and alkyl amine hexadecylamine for 7 days at 180°C. The results show that the growth process of the NanoUrchin occurs in stages, starting with a radial self-organized arrangement of lamina followed by the rolling of the lamina into nanotubes. The longest nanotubes are measured to be several micrometers in length with diameters of ~120 nm and hollow centers typically measured to be ~75 nm. The NanoUrchin have an estimated density of nanotubes of ~40 sr⁻¹. The tube walls comprise layers of vanadium oxide with the organic surfactant intercalated between atomic layers. The interlayer distance is measured to be 2.9 ± 0.1 nm and electron diffraction identified the vanadate phase in the VO_x nanocomposite as orthorhombic V₂O₅. These nanostructures may be used as three-dimensional composite materials and as supports for other materials.

1. Introduction

One-dimensional nanomaterials, such as nanotubes [1, 2], nanowires [3-5], and nanobelts or nanoribbons [6-8] have attracted considerable attention in the past decade because of their novel and useful physical properties leading to numerous potential applications. Besides the use of 1D nanostructures in electronics as functional components and interconnects in dense, high-speed circuits, they also have numerous applications among others in the design of ultra-small sensors, optical elements for optoelectronics, non-linear optical converters and information storage devices [9]. Although the majority of research and development has been based on carbon nanotubes, considerable attention is now being directed to transition metal nanostructures based on their metal oxides [10,11] which, due to their versatile chemical properties often modulable by changes in the oxidation state of in the metal coordination sphere, may lead to a variety of products and tunable materials [12,13].

Vanadium oxide based low dimensional products have been studied extensively. Starting from the laminar V_2O_5 xerogel [14] numerous two dimensional organic-inorganic intercalation products have been obtained [15].

Hydrothermal treatment (HT) of either of these laminar composites, especially those intercalated with long-chained amines or directly from the precursors, results in one dimensional tubular products with practical quantitative yields [16]. Many of these vanadate based nanostructures may be obtained in quantities of the order of grams. Together with the electrical and optical properties of vanadium oxide derivatives, this has encouraged its study as a potential new functional material. Applications such as optical switches [12], gas sensing [17] and as electrodes in Li rechargeable batteries [18] have been reported. The efficiency reached in the preparation of laminar and tubular nanostructures is necessary but not solely sufficient for integration of these materials in devices; specimens formed by ordered and dense arrays of uniform nanostructures are desired. Although there are numerous reports describing a wide range

of V₂O₅ based nanostructures, the possibility of realizing a three-dimensional array of one-dimensional nanostructures with high density and uniformity has remained elusive.

Here, we describe the nucleation and growth of hollow-centered spherical structures of micrometer-scale dimensions with a high-density, radially oriented array of hollow nanotubes that we have denominated ‘NanoUrchin’. Such high-density nanotube-containing structures are synthesized by a simple chemical route.

2. Experimental

2.1 Synthesis of Vanadium Oxide NanoUrchin

A solution of 10⁻³ mol of hexadecylamine (HDA) in 10 ml of pure ethanol, previously degassed by repetitive freeze-thaw cycling in an argon vacuum, was mixed with 2 × 10⁻³ mol vanadium (V) tri-isopropoxide (VOTPP). The yellow solution, obtained after vigorous stirring in an argon atmosphere for 1 h under argon atmosphere, was then hydrolized by adding 15 ml of doubly-deionized pure water. The orange suspension obtained after stirring for 24 h was characterized by FTIR and powder X-ray diffraction. The HT of the orange suspension was performed in a Teflon lined autoclave at 180°C for 7 days. From the resulting dark suspension a dark solid was separated, washed with pure ethanol and water, dried under vacuum (10⁻³ mm Hg) for 48 h at room temperature and stored under argon atmosphere. The final VO_x product has the composition V₂O₅(HDA)_{0.83} · 1.8H₂O. Analysis: Exp. (calculated for C_{13.28}H_{32.65}N_{0.83}O_{6.8}V₂), C: 39.06 (38.32); H: 8.05 (7.89); N: 2.56 (2.79).

2.2 Methods of Characterization

X-ray powder diffraction characterization was performed using a SIEMENS D5000 diffractometer (Cu-K_α, λ=1.5418 Å, operation voltage 40 kV, current 30 mA). The morphological characterization of the nanostructured products was performed by field emission scanning electron microscopy (FESEM) using a JEOL JSM-6700F FESEM operating at beam

voltages between 1-10 kV. Electron transparent specimens were prepared by ion-milling techniques and placed on a holey carbon support. Transmission electron microscopy (TEM) and electron diffraction (ED) were conducted using a JEOL 2000FX operating at 200 kV. The chemical composition of the samples was determined by elemental chemical analysis using a SISOONS model EA-1108 analyzer. The Fourier transform infrared (FTIR) spectra were recorded using a KBr pellet technique on a Perkin-Elmer series 2000 apparatus in the region 4000 to 450 cm^{-1} . Supplementary cathodoluminescence (CL) characterization was performed on a Gatan MonoCL 2 system operating at 10~kV.

3. Results and Discussion

Figure 1a shows the X-ray diffraction analysis of the product from the reaction of VOTPP with hexadecylamine in a 2:1 molar ratio under normal conditions followed by a hydrolysis process. The reaction leads to a mixture of products, among them unreacted V_2O_5 xerogel and a mesophase that, according to its $\{00l\}$ Bragg reflections, corresponds to the intercalation product of the amine into the vanadium oxide. The observed interlaminar distance, ~ 2.8 nm, which is larger than the amine molecular length (~ 2.12 nm) suggests a double layer of the amine oriented either perpendicularly to the V_2O_5 planes with interpenetrated alkyl chains or forming an angle with them [19]. As observed in the diffractogram shown in Fig. 1b, the HT of the reaction mixture leads to the formation of a pure mesophase formed by tubular species (*vide infra*) with interlaminar distances of ~ 3 nm. The composition of this mesophase, $\text{V}_2\text{O}_5(\text{HDA})_{0.83} \cdot 1.8\text{H}_2\text{O}$, agrees with the intercalation rate expected for a double layer of amine intercalated between the inorganic walls of the nanotubes which are in turn formed by a double layer of VO_4 tetrahedrons [20].

3.1 Structural Characterization of NanoUrchin

Figure 2 presents a typical SEM image of the VO_x NanoUrchin cluster. It is clearly observed that the cluster is composed of numerous spherical NanoUrchin of micrometer-sized dimensions. Survey micrographs show that over 95% of all individual NanoUrchin have diameters in the range 9-12 μm . From Fig. 2, it is evident that each NanoUrchin is covered with a high density of radially oriented pin-like structures.

A higher magnification SEM image of a single NanoUrchin is shown in Fig. 3. This image shows that the pin-like structures are in fact VO_x nanotubes that grow radially on the NanoUrchin. It is also evident from Figs. 2 and 3 that the NanoUrchin are three-dimensional, spherical, and typically $\sim 10\ \mu\text{m}$ in diameter. The structure of the nanotubes was examined in more detail using higher magnification SEM.

Figure 4 shows a higher magnification image of the nanotubes in an individual NanoUrchin. It is observed that the nanotubes have a regular column shape and are several micrometers long. Some open-ended nanotubes are also observed in Fig 4. Fig. 5 shows an SEM micrograph of two individual hollow nanotubes. The longest nanotubes are several micrometers in length and higher magnification SEM images (inset to Fig. 5) shows that the diameter of the open-ended tube is $\sim 120\ \text{nm}$, with hollow centers typically measured to be $\sim 75\ \text{nm}$ in diameter. Furthermore, the NanoUrchin also display a relatively high density of uniform nanotubes with a strikingly regular distribution. By estimating the density of nanotubes in a solid angle with a length of curvature of $1\ \mu\text{m}$, the nominal density of nanotubes in an individual NanoUrchin is estimated at $\sim 40\ \text{sr}^{-1}$, an unprecedented density of uniform hollow VO_x nanotubes.

3.2 Early Stages of NanoUrchin Formation

Figure 6 shows an SEM micrograph of an individual NanoUrchin at an early stage of formation. It is observed that the NanoUrchin structure possesses a reduced diameter, estimated

from several similar micrographs to be $\sim 1.5 - 3 \text{ }\mu\text{m}$. Each nanostructure is composed of numerous self-assembled lamina from which nanotubes nucleate and grow. The lamina emanate from one center and grow radially outwards. They slightly curve and gradually attenuate in growth towards the edges, resulting in 300-500 nm segments with thin edges of $\sim 100 \text{ nm}$ in dimension. The inset to Fig. 6 shows a fully spherical NanoUrchin that was quarter-sectioned by ion-milling, at the nucleation stage of nanotube growth. The inner portion is observed to be composed of numerous lamina, the majority of which have merged. In Fig. 7, a complete NanoUrchin is shown with its near face cleaved to show the central portion. The dotted circle highlights the central portion composed of self-assembled lamina. From the central region in Fig. 7, it is observed that the hollow axis of the nanotubes is parallel to that of the lamina resulting in their radial growth in all directions. It is also observed that the NanoUrchin are hollow-centered. In fact, imaging of several individual NanoUrchin indicates that each has a dedicated hollow center, an observation further confirmed by FIB images acquired during ion-milling procedures.

3.3 High-Resolution Electron Microscopy of the Nanotubes

Further structural characterization was performed with TEM, where NanoUrchin structures were placed on a holey carbon support. Figure 8 shows a relatively low magnification displaced aperture dark field image of typical regions of the sample where it is possible to observe several individual NanoUrchin. The electron diffraction pattern in the inset shows prominent polycrystalline diffraction with d -spacings matching the (200), (001) and (110) reflections of orthorhombic V_2O_5 , corresponding to A, B and C in Fig. 8 respectively. This evidence clearly shows that there is no preferred crystal orientation for the NanoUrchin bulk.

The diffuse nature of the electron diffraction peaks is indicative of the presence of small domain sizes. The presence of these small crystallites was conclusively verified by TEM measurements, shown in Fig. 9, of a relatively large sample area, *i.e.* several nanotubes. The

bright field (Fig. 9a) and dark field (Fig. 9b) images are taken from the same sample area. Phase contrast effects were also utilized to enhance the visibility of fine crystallites contained within each hollow nanotube, seen at 'V'. Conclusive evidence for the presence of individual crystallites is presented in the dark field image where multiple equiaxed grains are observed varying in diameter from 2 – 5 nm. What is noteworthy about these images is that the contrast verifies the thin and thick vanadate layers showing the beginning of a rolling-up mechanism, which are precursors to the final rolled nanotube structure discussed later.

Individual parts of the NanoUrchin were examined in more detail. In particular, HRTEM data was acquired for nanotubes both at early and advanced stages of growth. Figure 10 shows a high resolution TEM image of an early stage nanotube. It can be observed that the sidewall regions are characterized by the 2.85 nm spacing of the lattice fringes. A particular characteristic of these nanotubes is the presence of half-spacing within the lattice planes. For early stage nanotubes, the internal hollow diameter decreases along its length, observed here to taper down to ~5 nm in diameter at the open end. The central core of the nanotube, seen at 'B' is observed to be hollow and extends to the very tip. The measured lattice spacing of 2.85 nm corresponds to the *d*-spacing of the (100) crystal planes of V₂O₅ in the VO_x nanocomposite, confirming that the nanotubes have preferential growth in the [100] direction.

Overall, the tube is structurally uniform but there is evidence of lattice plane termination dislocations at 'C' in Fig. 10. Although not shown here, further high-resolution images show similar dislocations caused by the additional lattice plane inclusions. Details on these observations will be published elsewhere.

A high resolution TEM image of a fully developed nanotube is presented in Fig. 11. The micrograph highlights its tubular nature; the constant diameter hollow center extends to the tip of the nanotube and has a diameter of ~20 nm. As in the previous case, the sidewalls of the tube are composed of regularly spaced lattice planes with the same interplane spacing as found for

Fig. 10. A lattice plane inclusion dislocation is also observed at 'U', where an additional plane of atoms is observed, in contrast to Fig. 10, where a plane of atoms terminated before the end of the tube. Such characteristic dislocations are the only crystallographic defects noted in these nanotubes.

3.4 Infra-Red Spectroscopic Characterization

Figure 12 shows the FTIR spectrum obtained for the NanoUrchin. From previous reports [19,20] it was observed that the V_2O_5 xerogel (prior to the HT) displays three major absorption peaks at 530, 765, and 1012 cm^{-1} [21]. Our FTIR measurements of the nanocomposite after HT show five characteristics bands for VO_x . Spectral analysis shows that these frequencies correspond to the V=O bond of the vanadyl oxygen ($999, 949\text{ cm}^{-1}$), V-O-V asymmetric stretching (797 cm^{-1}), and V-O-V symmetric stretching ($587, 529\text{ cm}^{-1}$) mixed with deformation vibrations of the vanadium-oxygen polyhedra, respectively [22,23].

The NanoUrchin nanocomposite also exhibits characteristics bands at 3135 and 3452 cm^{-1} attributed to the N-H vibrational stretching mode of the hexadecylamine surfactant used during the synthesis of the nanocomposite [24]. Intense bands resulting from surfactant molecules are observed at 2917 and 2852 cm^{-1} , related to the axial stretching of aliphatic C-H. Other notable bands are located at 1461 cm^{-1} , related to in-plane symmetric angular deformations of CH_2 species, as well a band at 735 cm^{-1} corresponding to the C-H bending mode of the methylene group in the surfactant. The band at 1610 cm^{-1} is attributed to the N-H bending mode of the surfactant and the H-O-H bending mode of the water molecule is also observed [24,25]. The bands at 949 and 999 cm^{-1} correspond to the vibrational V=O stretching mode (vanadyl oxygen) and are considered to be related to the two equivalent V=O groups reported for V_2O_5 nanorods [22,23]. Indeed, the calculated interatomic distances are 1.58 \AA for $\alpha\text{-}V_2O_5$ and 1.55 \AA for $\gamma\text{-}V_2O_5$, respectively. The observation of H-O-H vibrational modes in the region $3890\text{-}3640\text{ cm}^{-1}$ and a weak signal with a maximum at 1796 cm^{-1} indicates a detectable presence of remnant water

molecules within the NanoUrchin. This observation is in marked contrast to findings by Chen *et al.* [25] who did not detect the presence of water molecules in their nanotubes, as a result normally consistent with nanorods and solid nanofibers of V_2O_5 [22,24].

3.5 Growth Stages of the NanoUrchin

Based on these observations, we summarize the probable growth stages of the NanoUrchin, outlined in Fig. 13. Since we observe the NanoUrchin to be hollow-centered, the initial stage is presumed to be that of a ‘linking’ of the lamina of the VO_x nanocomposite (Fig. 13a) in the presence of the amine that is in excess outside of the host, represented by stage **1** in Fig. 13. The second stage of growth, **2**, is the self-organized arrangement of fan-like laminar structures (Fig. 13b) in a radial fashion forming a spherical structure (Fig. 13c) with a hollow center. These lamina arrange themselves radially from the core, presumably due to the presence of the amine molecules, while maintaining a constant degree of edge curvature. Numerous lamina appear to self-assemble into an urchin-like structure and each laminar structure seems to reach a certain size before apparent weaving occurs. During HT, the precursors become crystallized ordered lamina. The third stage, illustrated by **3**, is the rolling of hollow, open-ended VO_x nanotubes from the thin, curved edges of the lamina evidenced in the SEM images in (d) and (e) in Fig. 13. The rolling mechanism is similar to that reported by Chen *et al.* [25] and Trasobares *et al.* [26] where rolling of vanadate layers and ‘wings’ are observed in each respective case. The growth direction of the hollow-axis of the nanotubes is radially toward the core of the structure. Elemental analysis and the X-ray powder patterns show that there is, even at this stage, a sufficient quantity of amine in excess during the HT to allow the intercalation and rolling of the tubes and the self-organization of the lamina. The condensation process of during HT not only brings about the ordered arrangement of the lamina but also loosens the curved edges of the sheets of VO_x allowing the initiation of layer rolling, forming the nanotubes [25]. At stage **4**, the nanotubes are observed to have rolled into tubes with lengths of several micrometers and the

overall diameter of the NanoUrchin has increased ~ 3 -fold, presumably due to continuing attachment of VO_x lamina. Thus, we observe a fully developed NanoUrchin: a spherical, hollow-centered, micrometer sized structure (Fig. 13f), containing hundreds of radially oriented VO_x nanotubes.

4. Conclusions

We have reported the observation of urchin-like nanostructured nanocomposite based on the intercalation of a neutral surfactant into vanadium oxide. Each NanoUrchin consists of a spherical high-density radial array of nanotubes, successfully synthesized by a simple chemical route using an ethanolic solution of vanadium tri-isopropoxide and alkyl amine hexadecylamine. The initiation of the growth of the NanoUrchin comprises a radial self-organized arrangement of lamina followed by the rolling of the lamina into nanotubes. The nanotube density on these spherical NanoUrchin structures is estimated at $\sim 40 \text{ sr}^{-1}$.

The longest nanotubes are measured to be several micrometers in length with diameters of $\sim 120 \text{ nm}$ and hollow centers typically measured to be $\sim 75 \text{ nm}$ and high resolution electron microscopy studies show highly ordered structures with an inter atomic plane distance of 2.85 nm . Electron diffraction shows that the vanadate constituent of the VO_x nanocomposite is primarily composed of orthorhombic V_2O_5 .

Spectroscopic investigations show detectable levels of surfactant within the structures, which according to observed interlaminar distances, is arranged as a bilayer between oxide layers. Such functionalized oxide nanostructures may be potentially useful in reinforcing composite materials or in further modifying other nanostructures. With a fuller understanding of these processes, a greater control over the growth process, resultant morphology and potential material systems will eventually be realized.

Acknowledgements

The support of the Science Foundation Ireland (SFI) under investigator award 02/IN.1/I172, the network of excellence PHOREMOST, the University of Chile, the Universidad Tecnológica Metropolitana and FONDECYT (Grants 1050344, 1030102, 7050081, 1050788) are gratefully acknowledged. The authors also thank Dr. Y. Lanyon for conducting ion-milling of selected samples.

References

- [1] Iijima, S. *Nature* **1991**, 354, 56.
- [2] Ajayan, P. M.; Iijima, S. *Nature* **1992**, 358, 23.
- [3] Morales, A. M.; Lieber, C. M. *Science* **1998**, 279, 208.
- [4] Zhang, Y. F.; Tang, Y. H.; Wang, N.; Yu, D. P.; Lee, C. S.; Bello, I.; Lee, S. T. *Appl. Phys. Lett.* **1998**, 72, 1835.
- [5] Holmes, J. D.; Johnston, K. P.; Doty, R. C.; Korgel, B. A. *Science* **2000**, 287, 1471.
- [6] Pan, Z. W.; Dai, Z. R.; Wang, Z. L. *Science* **2001**, 291, 1947.
- [7] Gao, Y. H.; Bando, Y.; Sato, T. *Appl. Phys. Lett.* **2001**, 79, 4565.
- [8] Shi, W. S.; Peng, H. Y.; Wang, N.; Li, C. P.; Xu, L.; Lee, C. S.; Kalish, R.; Lee, S. T. *J. Am. Chem. Soc.* **2001**, 123, 11095.
- [9] Xia, Y. N.; Yang, P. D.; Sun, Y. G.; Wu, Y. Y.; Mayers, B.; Gates, B.; Yin, Y. D.; Kim, F.; Yan, H. Q. *Adv. Mater.* **2003**, 15, 353.
- [10] Soga, N.; Senna, M. *Sol. State Ion.* **1993**, 63-65, 471.
- [11] Gomez-Romero, P. *Adv. Mater.* **2001**, 13, 163.
- [12] Xu, J. F.; Czerw, R.; Webster, S.; Carroll, D. L.; Ballato, J.; Nesper, R. *Appl. Phys. Lett.* **2002**, 79, 1711.
- [13] Gomez-Navarro, C.; de Pablo, P. J.; Colchero, J.; Fan, Y.; Burghard, M.; Gomez-Herrero, J.; Baro, A. M. *Nanotechnology* **2003**, 14, 134.
- [14] Ruiz-Hitzky, E. 'Organic-Inorganic Materials: From Intercalations to Devices': Chapter 2, in: Gomez-Romero, P; Sanchez, C. eds. *Functional Hybrid Materials* **2004** Wiley-VCH Verlag GmbH.
- [15] Gimenes, M. A.; Profeti, L. P. R.; Lassali, T. A. F.; Graeff, C. F. O.; Oliveira, H. P. *Langmuir* **2001**, 17, 1975.

- [16] Patzke, G. R.; Krumeich, F.; Nesper, R. *Angew. Chem. Int.* **2002**, *41*, 2446.
- [17] Kim, G. T.; Muster, J.; Krstic, V.; Park, J. G.; Park, Y. W.; Roth, S.; Burghard, M. *Appl. Phys. Lett.* **2000**, *76*, 1875.
- [18] Ando, M.; Kadono, K.; Haruta, M.; Sakaguchi, T.; Miya, M. *Nature* **1995**, *374*, 625.
- [19] Lavayen, V.; Santa Ana, M. A.; Seekamp, J.; Sotomayor, C. M.; Benavente, E.; González, G. *Mol. Cryst. Cryst. Liq.* **2004**, *416*, 49.
- [20] Malta, M.; Louarn, G.; Errien, N.; Torresi, R. *Electrochem. Commun.* **2003**, *5*, 1011.
- [21] Souza Filho, A. G.; Pereira, O. P.; Santos, E. J. G.; Mendes Filho, J.; Alves, O. L. *Nano Lett.* **2004**, *4*, 2099.
- [22] Malta, M.; Torresi, R.; Louarn, G.; Errien, N. *Electrochim. Acta* **2005**, *50*, 5009.
- [23] Pinna, N.; Willinger, M.; Weiss, K.; Urban, J.; Schogl, R. *Nano Lett.* **2003**, *3*, 1131.
- [24] Chen, W.; Mai, L. Q.; Peng, J. F.; Xu, Q.; Zhu, Q. Y. *J. Mater. Sci.* **2004**, *39*, 2625.
- [25] Chen, X.; Sun, X.; Li, Y. *Inorg. Chem.* **2002**, *41*, 4527.
- [26] Trasobares, S.; Ewels, C. P.; Birrell, J.; Stephan, O.; Wei, B. Q.; Carlisle, J. A.; Miller, D.; Keblinski, P.; Ajayan, P. M. *Adv. Mater.* **2004**, *16*, 610.

Figure Captions

Fig. 1 X-Ray diffraction analysis of the reaction mixture of VOTPP with HDA (a) prior to HT and (b) after HT.

Fig. 2 FESEM images of a typical NanoUrchin cluster. NanoUrchin structures are $\sim 10\text{ }\mu\text{m}$ in diameter and are most often observed in such dense groups.

Fig. 3 FESEM image of an individual NanoUrchin. This fully-grown NanoUrchin measures $12\text{ }\mu\text{m}$ in diameter and is covered in VO_x nanotubes with a volumetric density of $\sim 40\text{ sr}^{-1}$.

Fig. 4 FESEM image of the nanotube packing on the NanoUrchin. All tubes grow radially in all directions from the center of the NanoUrchin structure.

Fig. 5 High magnification FESEM image of individual nanotubes at the outer region of the NanoUrchin. The nanotubes are several micrometers in length, hollow and open ended. Inset: FESEM image of a nanotube cross-section. Such nanotubes are typically 100-120 nm in diameter with inner open diameters of 70-80 nm.

Fig. 6 FESEM image of the early stage of NanoUrchin formation. Lamina structures are clearly observed from which nanotubes nucleate and grow. Inset: A full NanoUrchin at an early growth stage that was quarter-sectioned by ion-milling where the lamina structure are visible.

Fig. 7 Cross-sectional FESEM micrograph of a fully developed NanoUrchin. The dotted circle indicates the area where the lamina are present, outside of which the growth of nanotubes is observed.

Fig. 8 Displaced aperture dark field TEM image of the NanoUrchin. Individual nanotubes are highlighted at P and Q. Inset: Associated electron diffraction pattern of the bulk nanocomposite.

Fig. 9 Bright field (a) and dark field (b) through focal TEM micrographs of several nanotubes from a single NanoUrchin. Examples of equiaxed crystallites can be found at 'D' and 'E' in (a). Evidence for branching of nanotubes is presented at 'W' in (b). Hollow centers of individual nanotubes are highlighted at (V).

Fig. 10 High resolution TEM image of an early stage nanotube. Lattice planes are clearly resolved (A) and have an measured lattice spacing $a = 2.85$ nm. The hollow center (B) extends to the tip of the nanotube. A lattice plane termination dislocation is also observed (C).

Fig. 11 High-resolution bright field TEM image of a fully developed nanotube acquired at Scherzer defocus. Lattice planes are clearly resolved at the sidewall regions. The hollow center extends to the tip of the nanotube. A lattice plane inclusion dislocation is also observed (U).

Fig. 12 FTIR transmittance spectrum, averaged from 300 scans, of the VO_x NanoUrchin nanocomposite acquired at room temperature between 4000 and 450 cm^{-1} .

Fig. 13 Schematic summary of the growth stages of VO_x NanoUrchin.

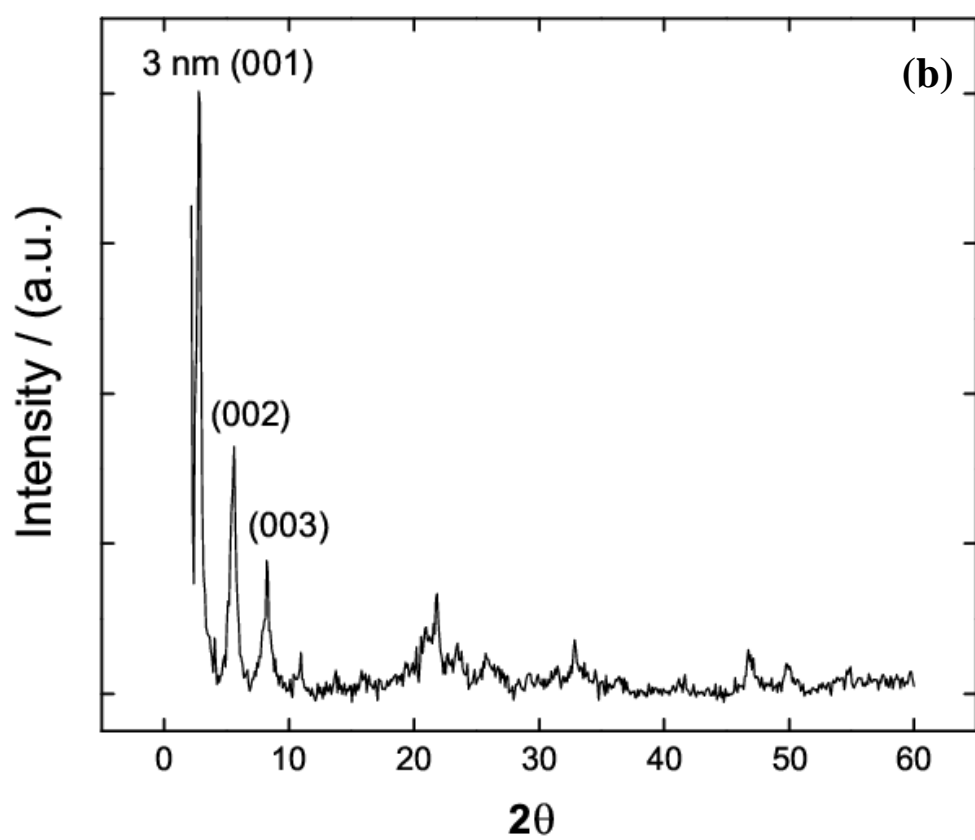
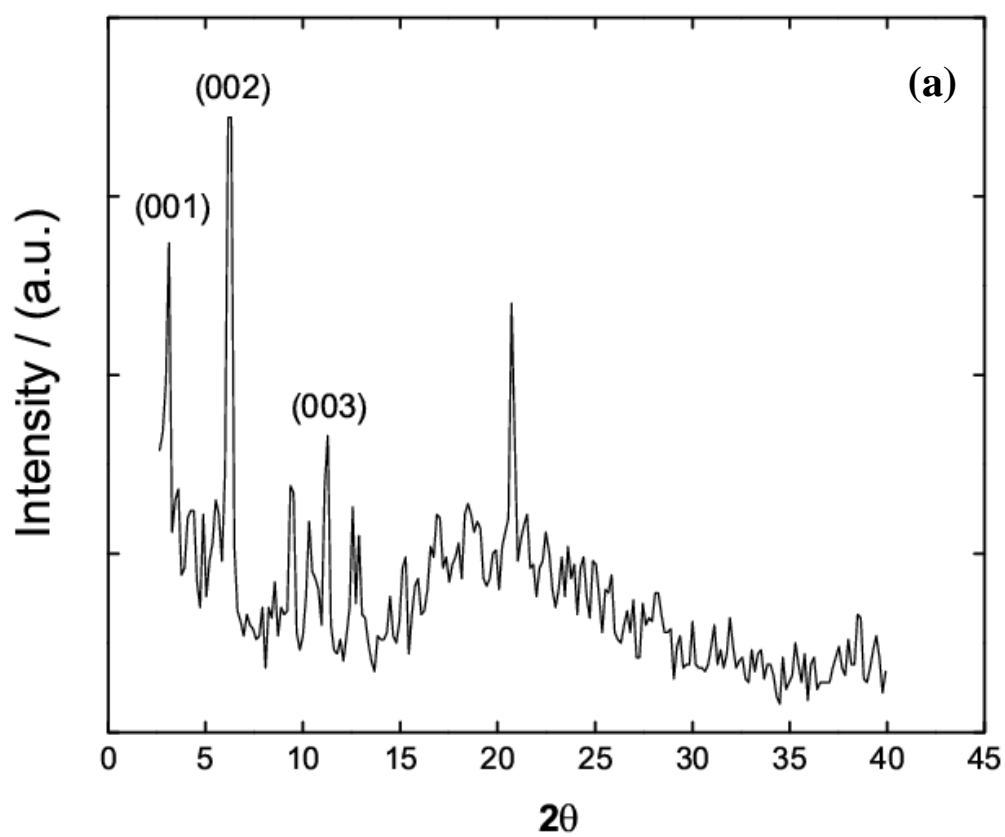


Fig. 1

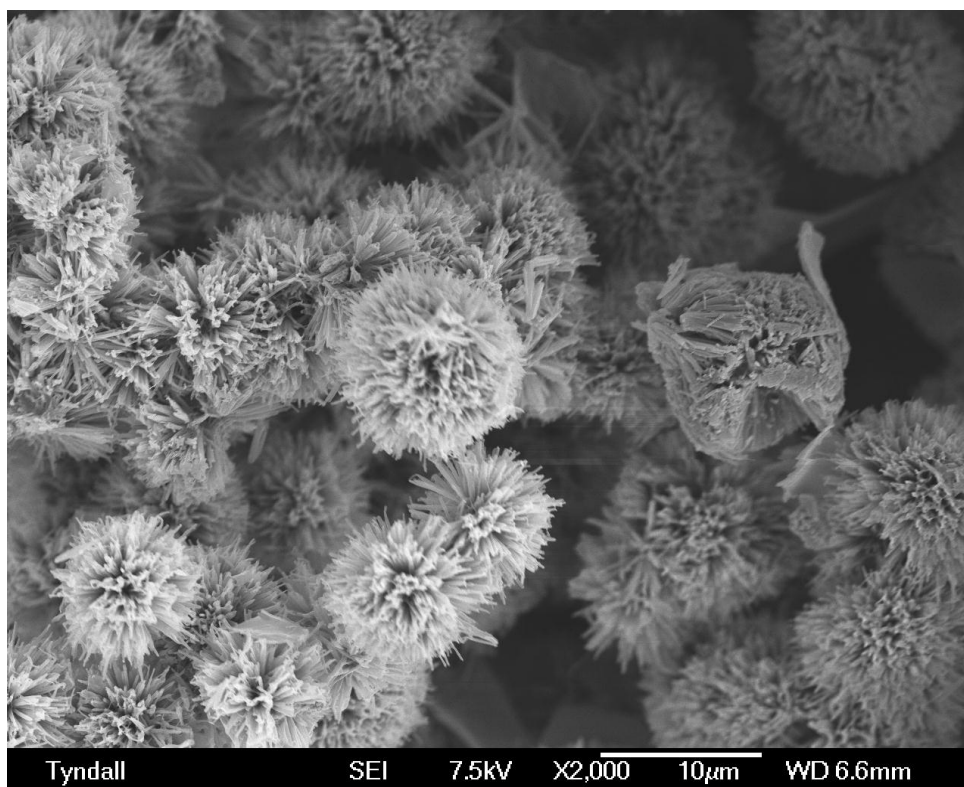
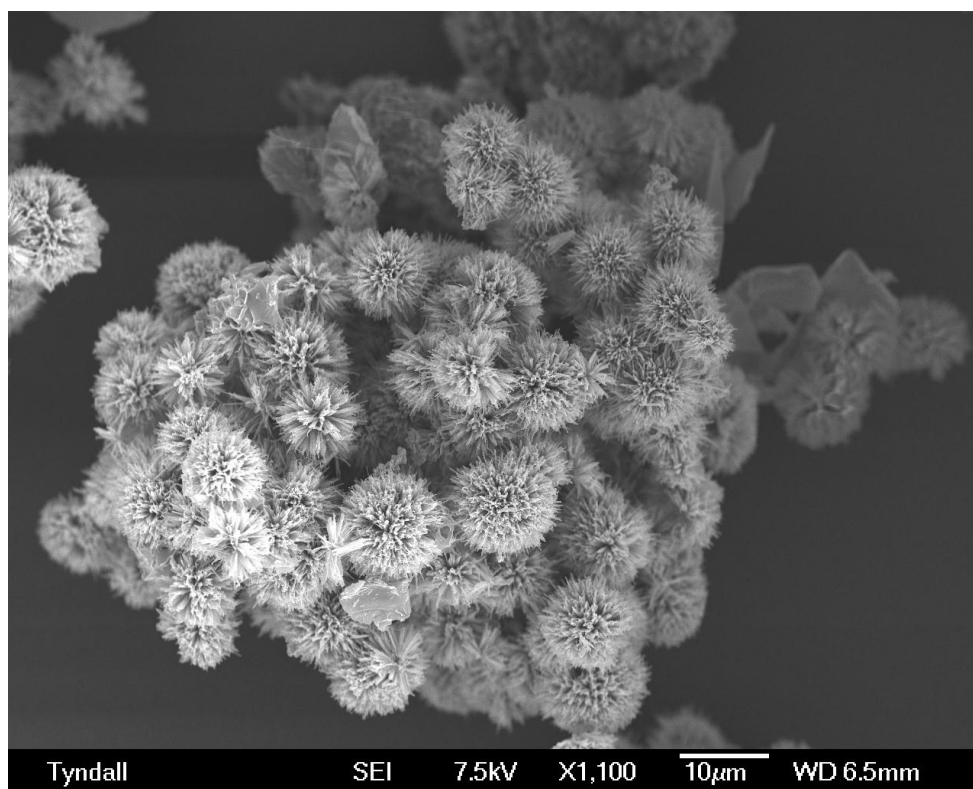


Fig. 2

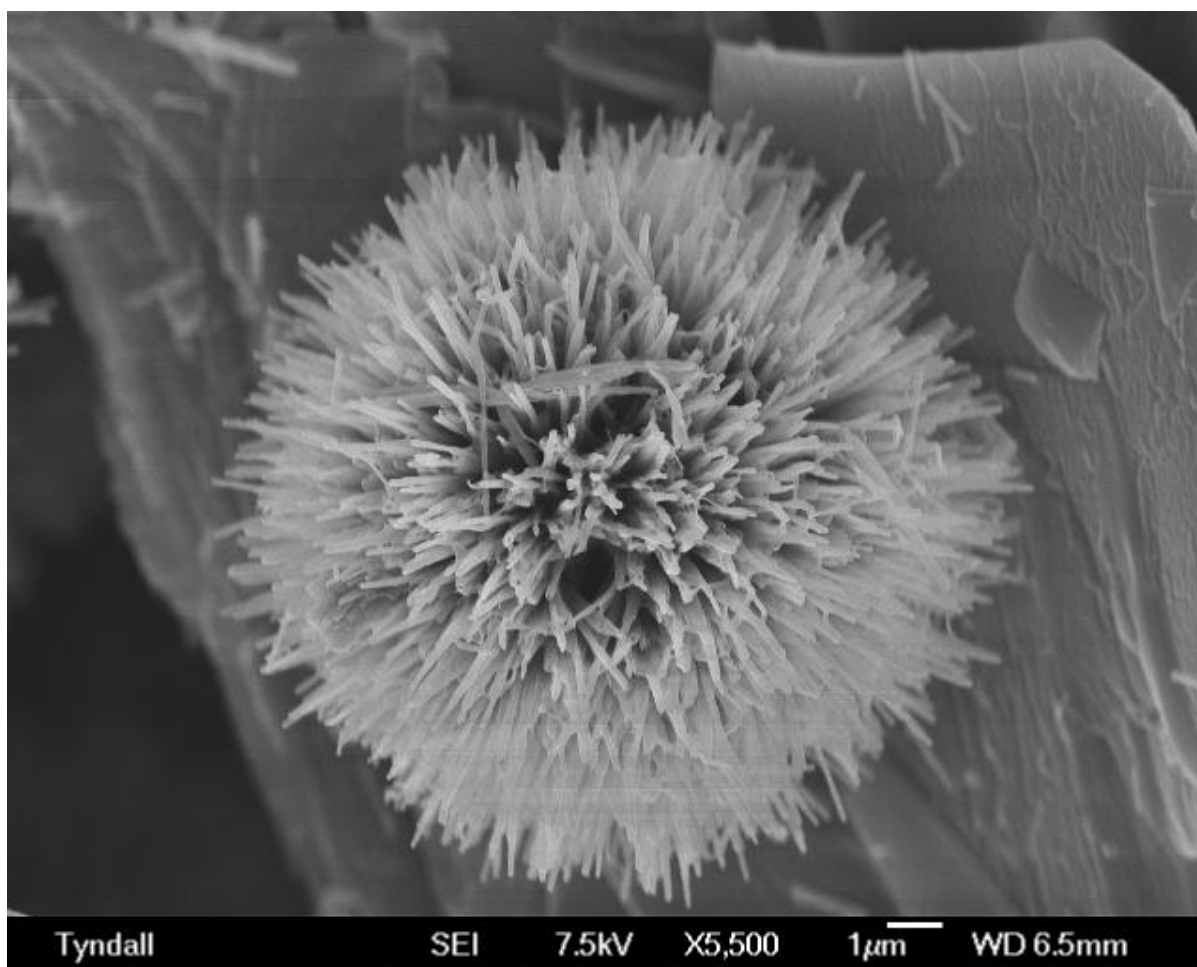


Fig. 3

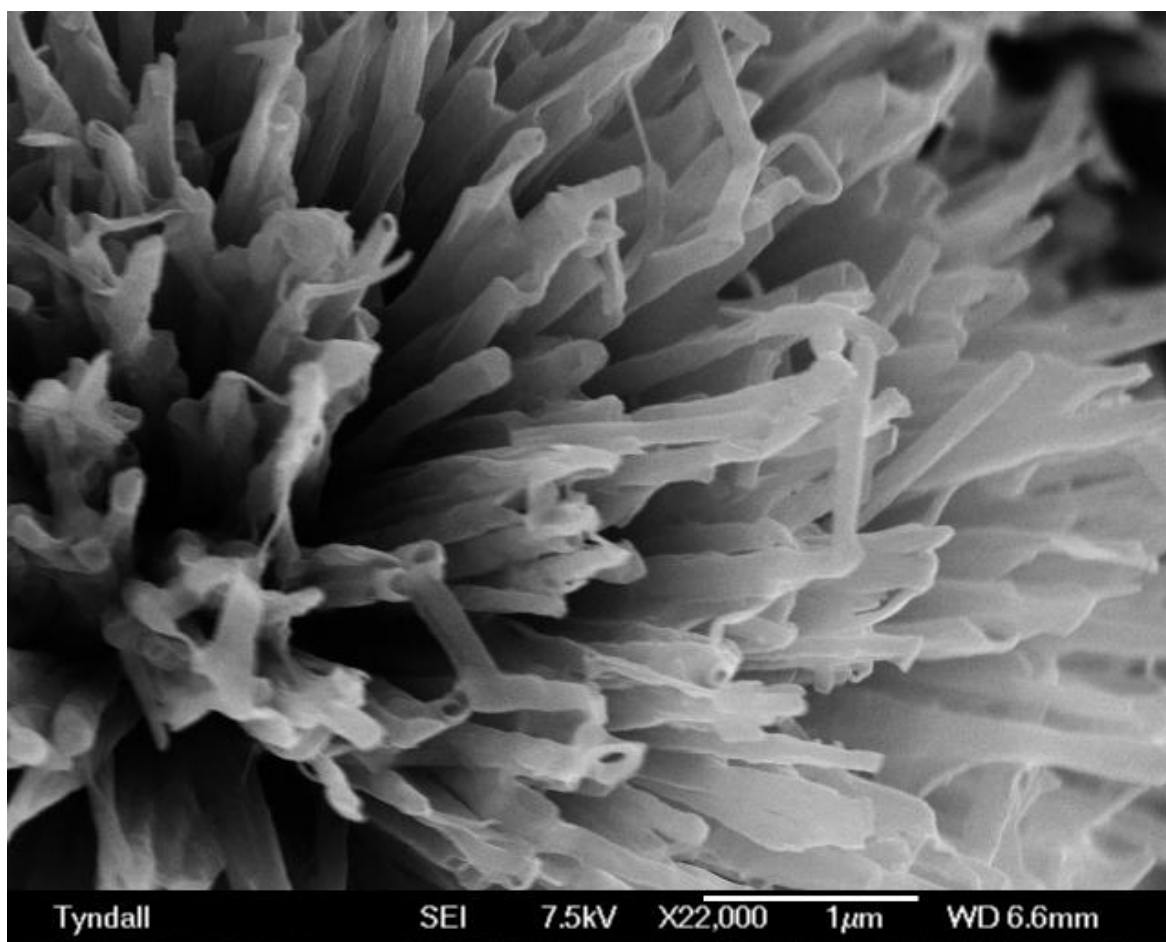


Fig. 4

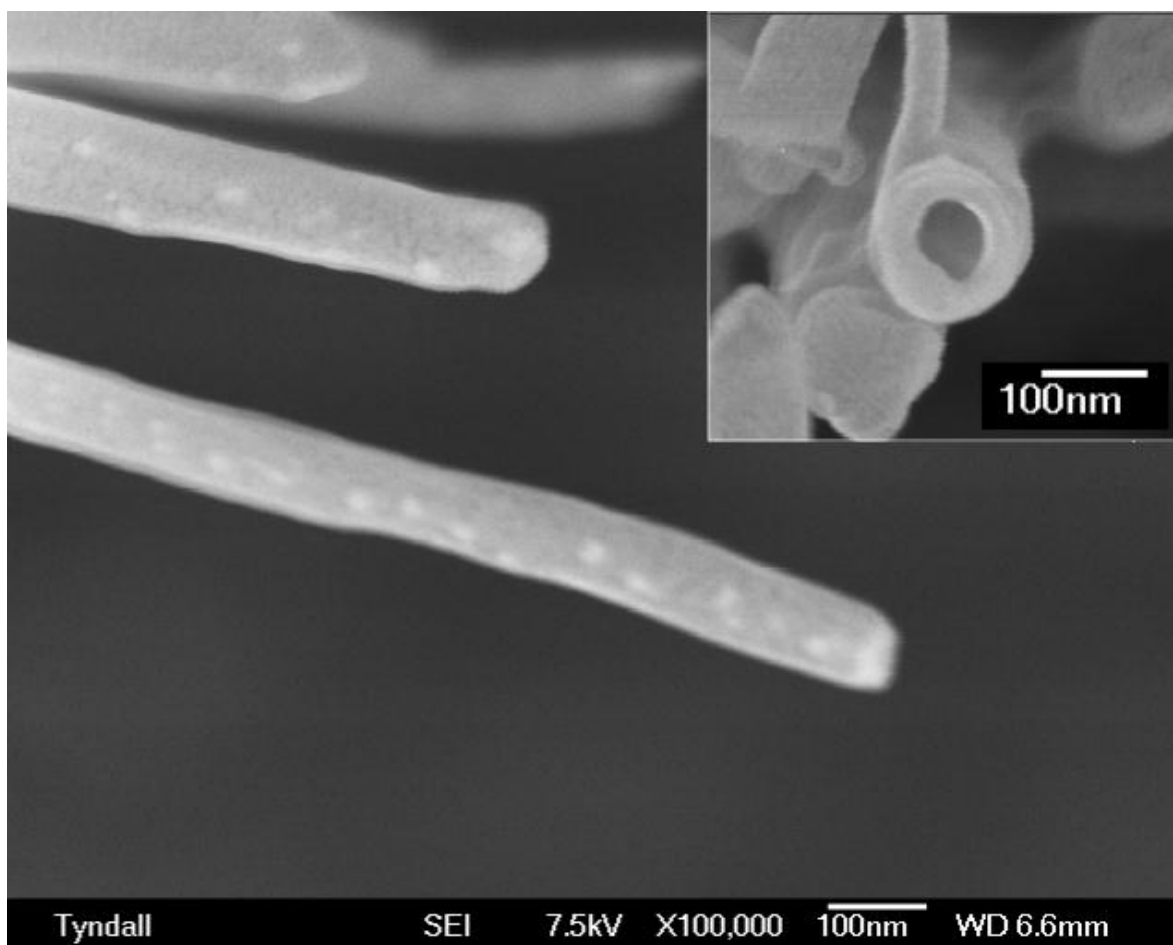


Fig. 5

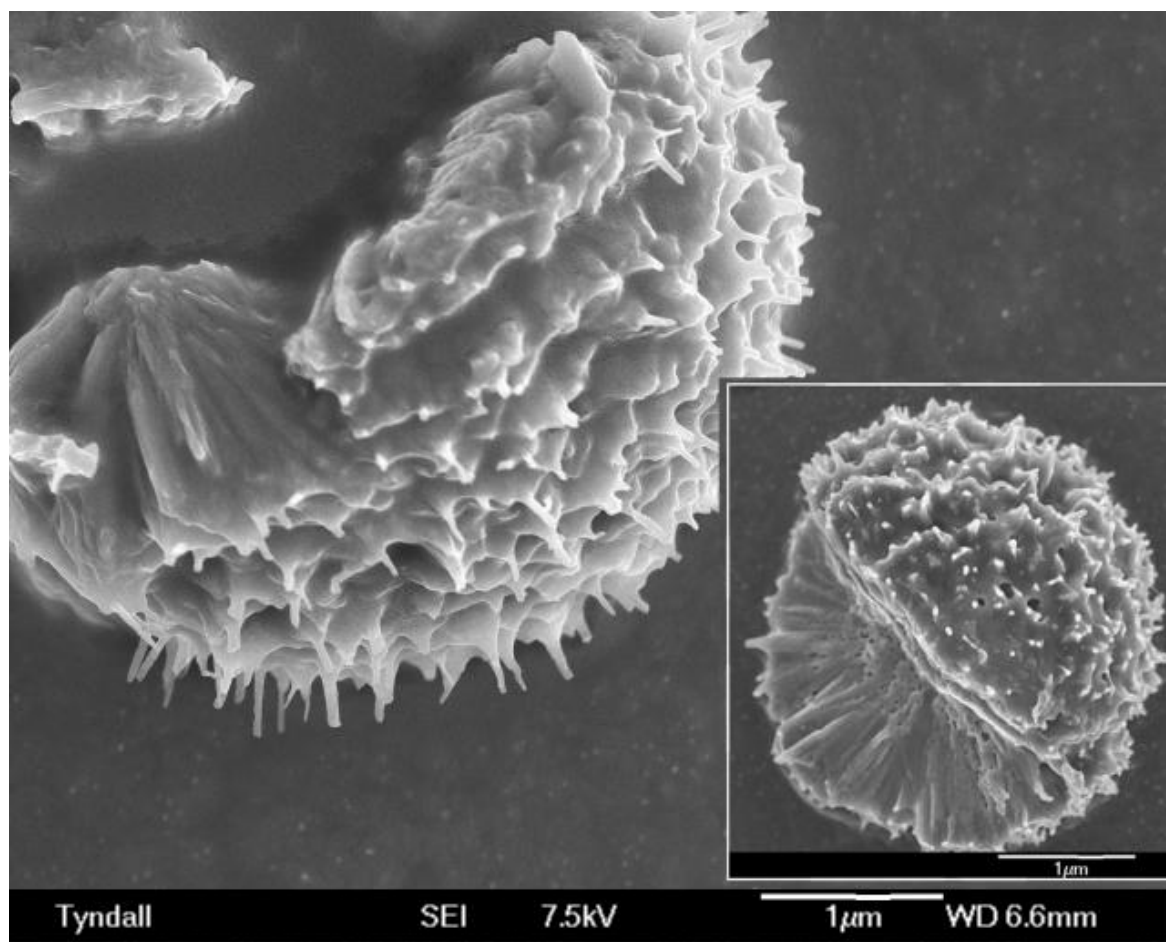


Fig. 6

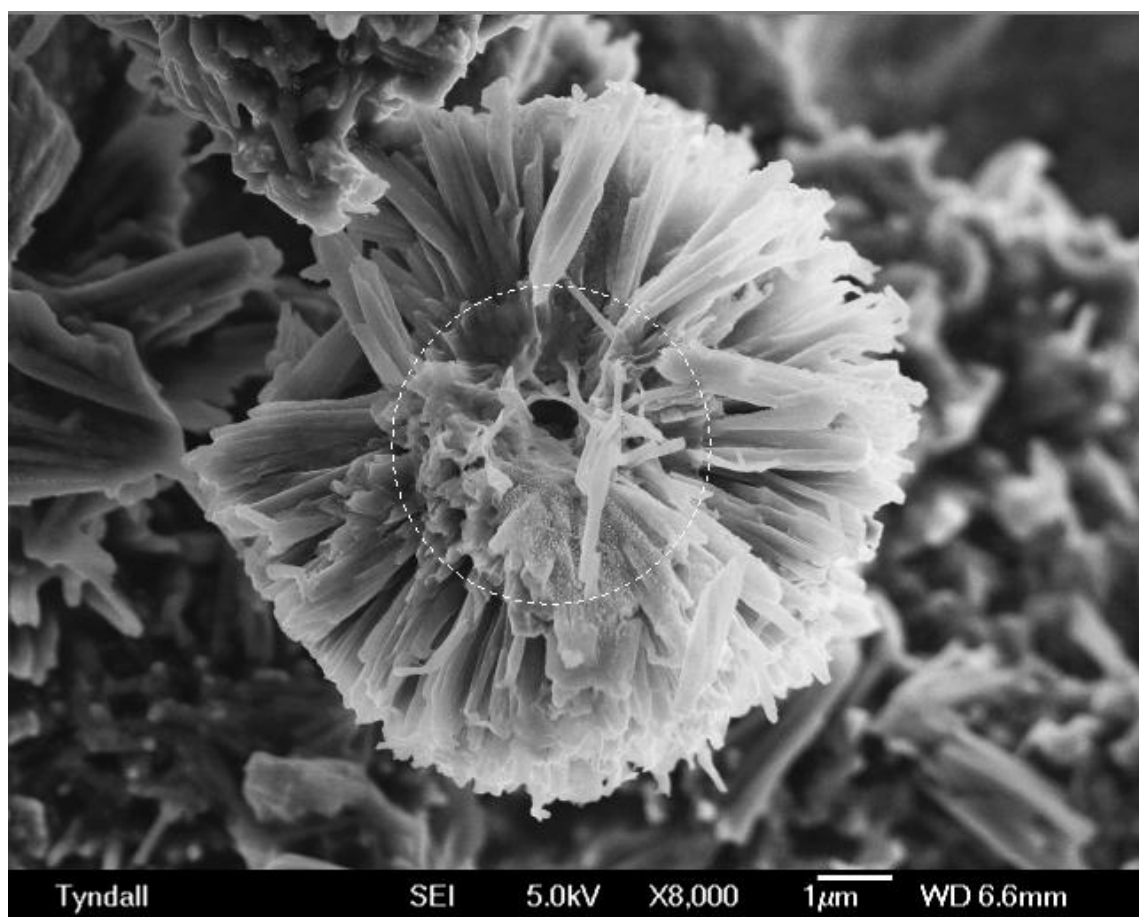


Fig. 7

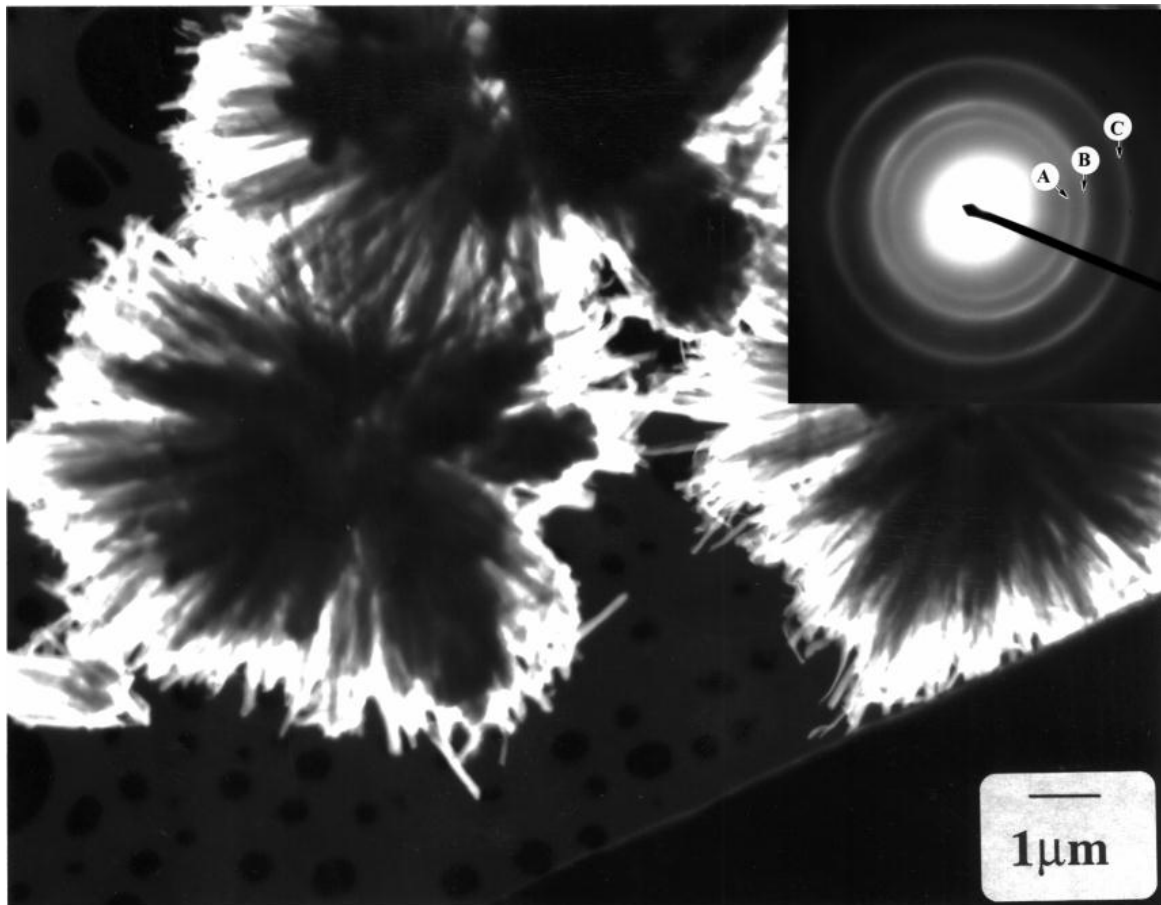


Fig. 8

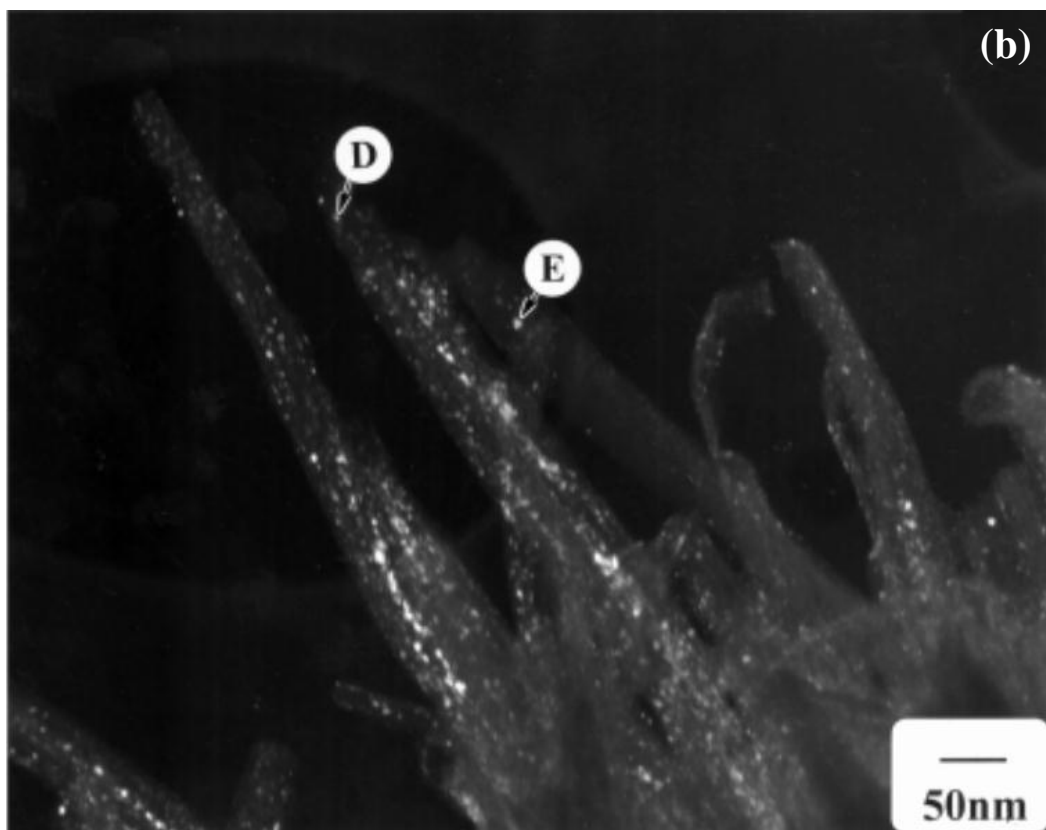
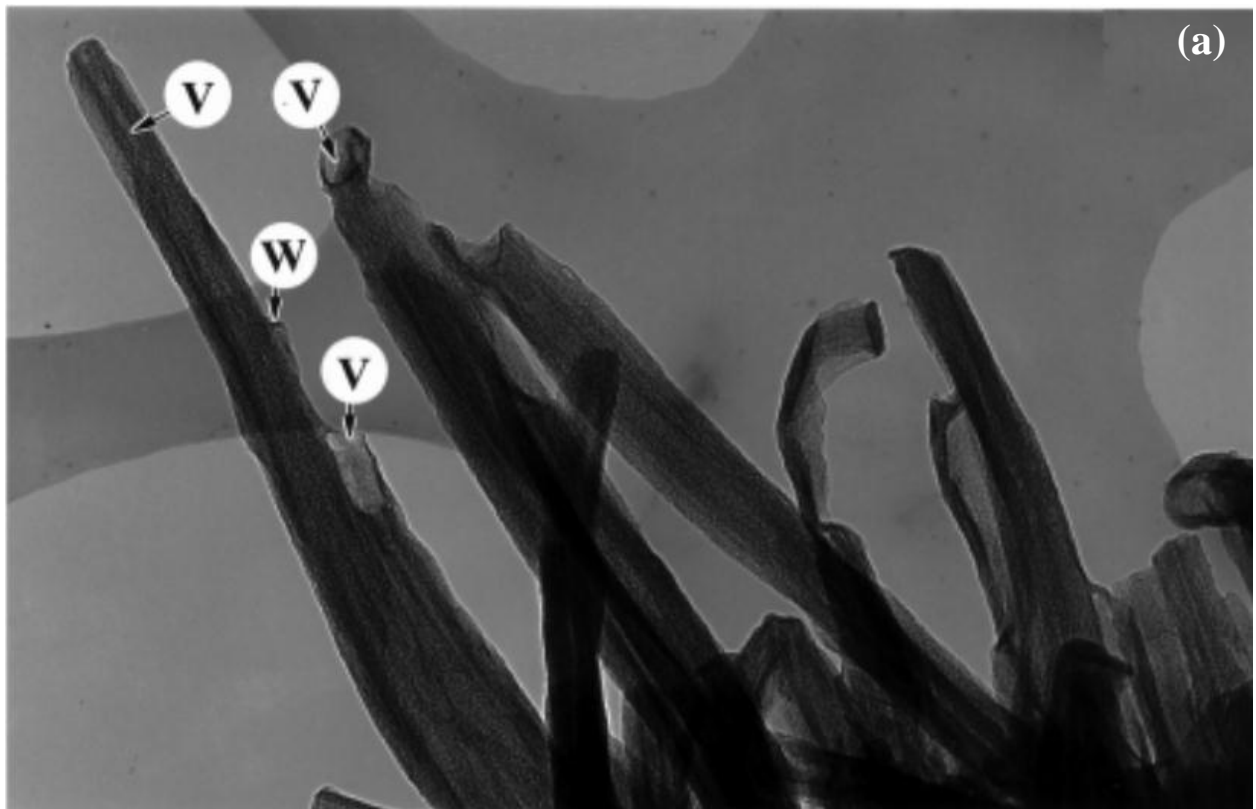


Fig. 9

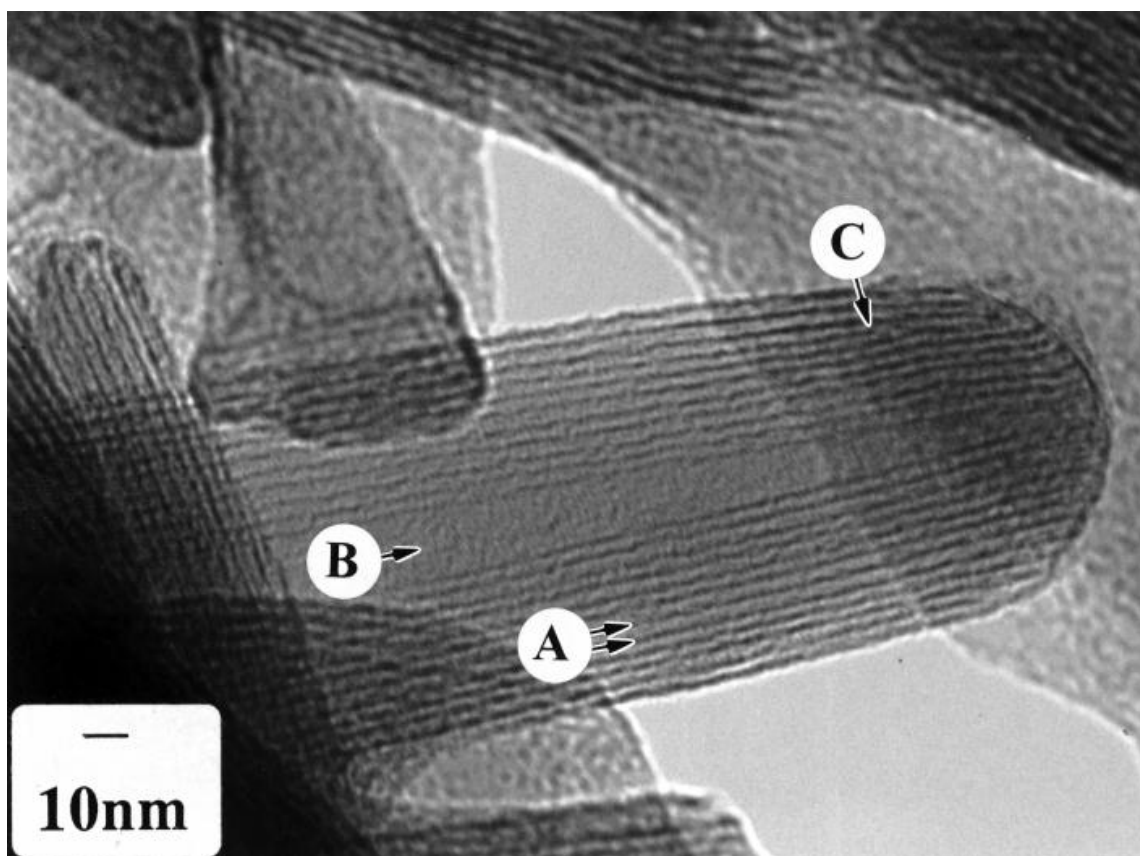


Fig. 10

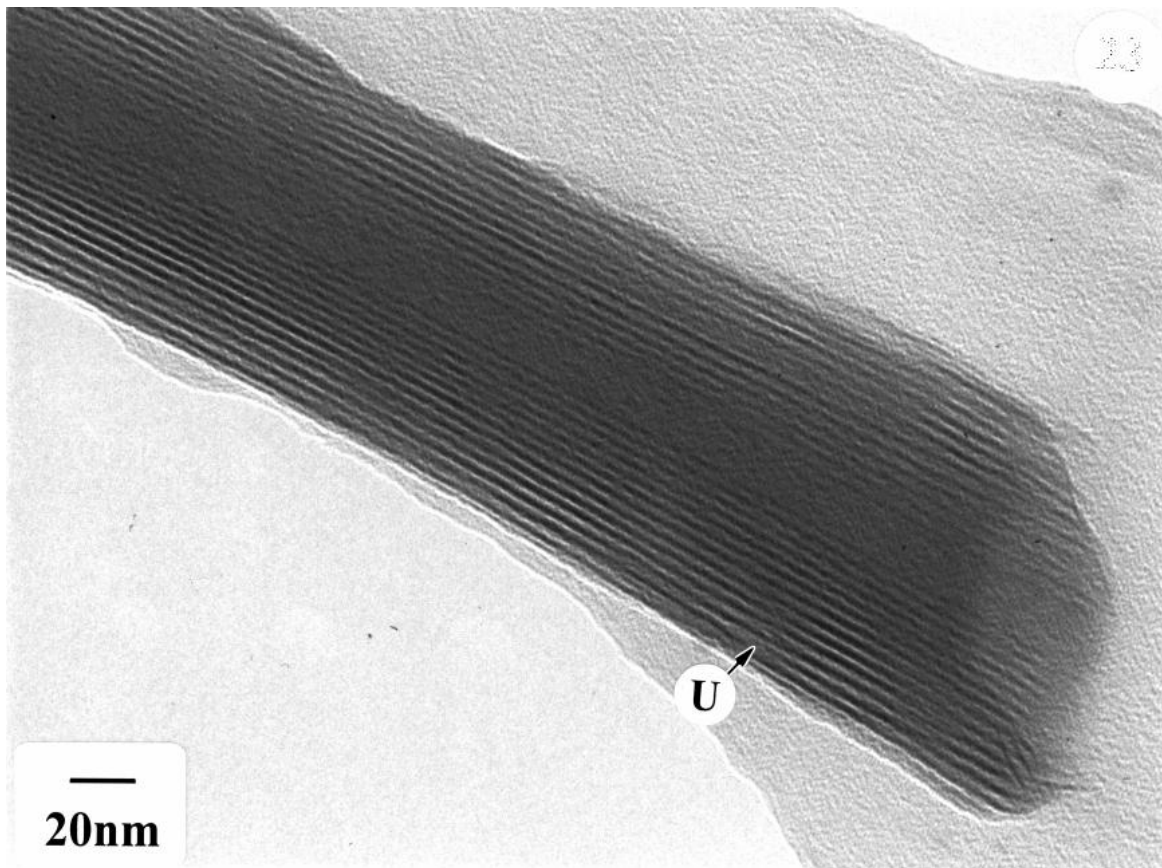


Fig. 11

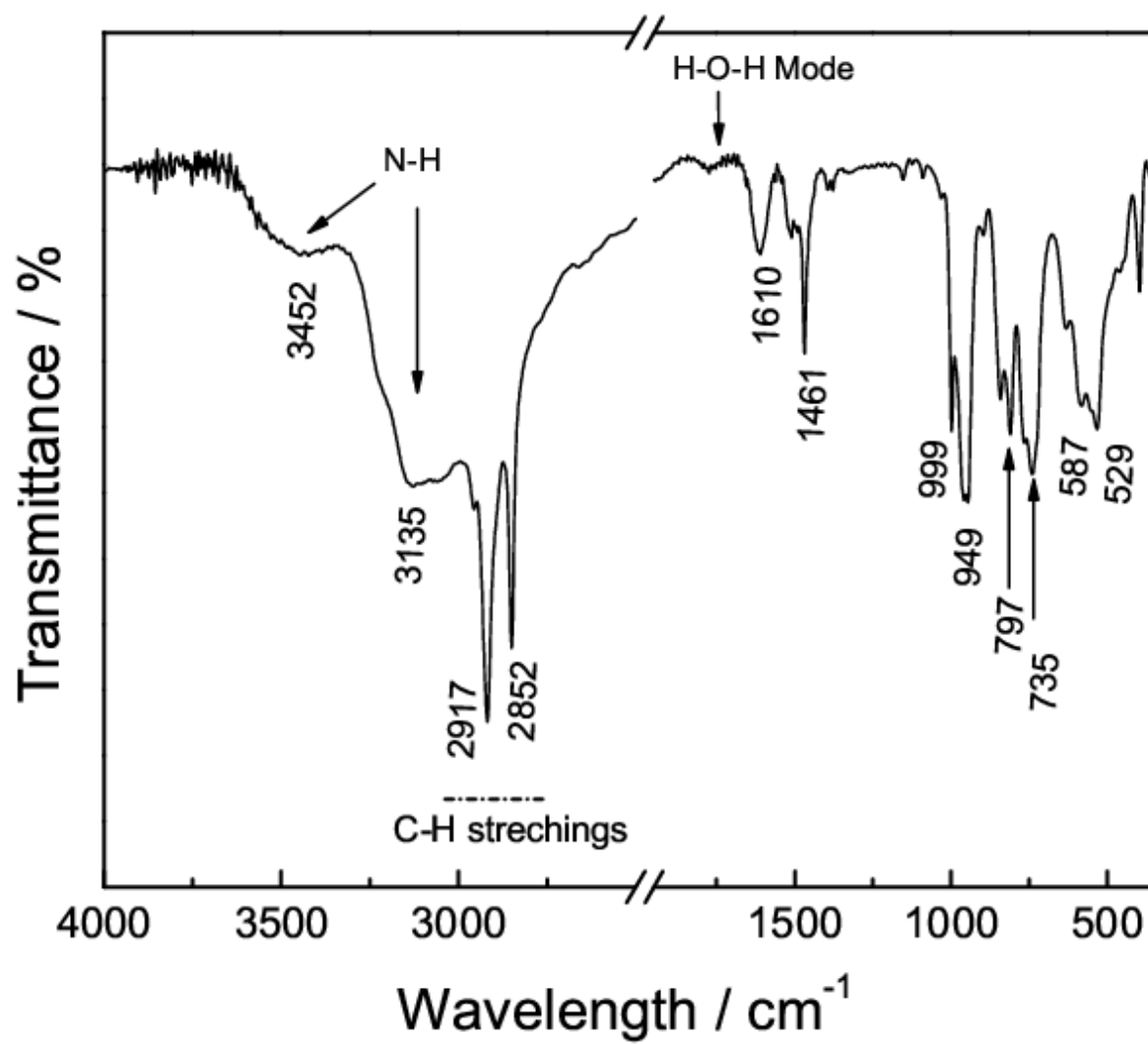


Fig. 12

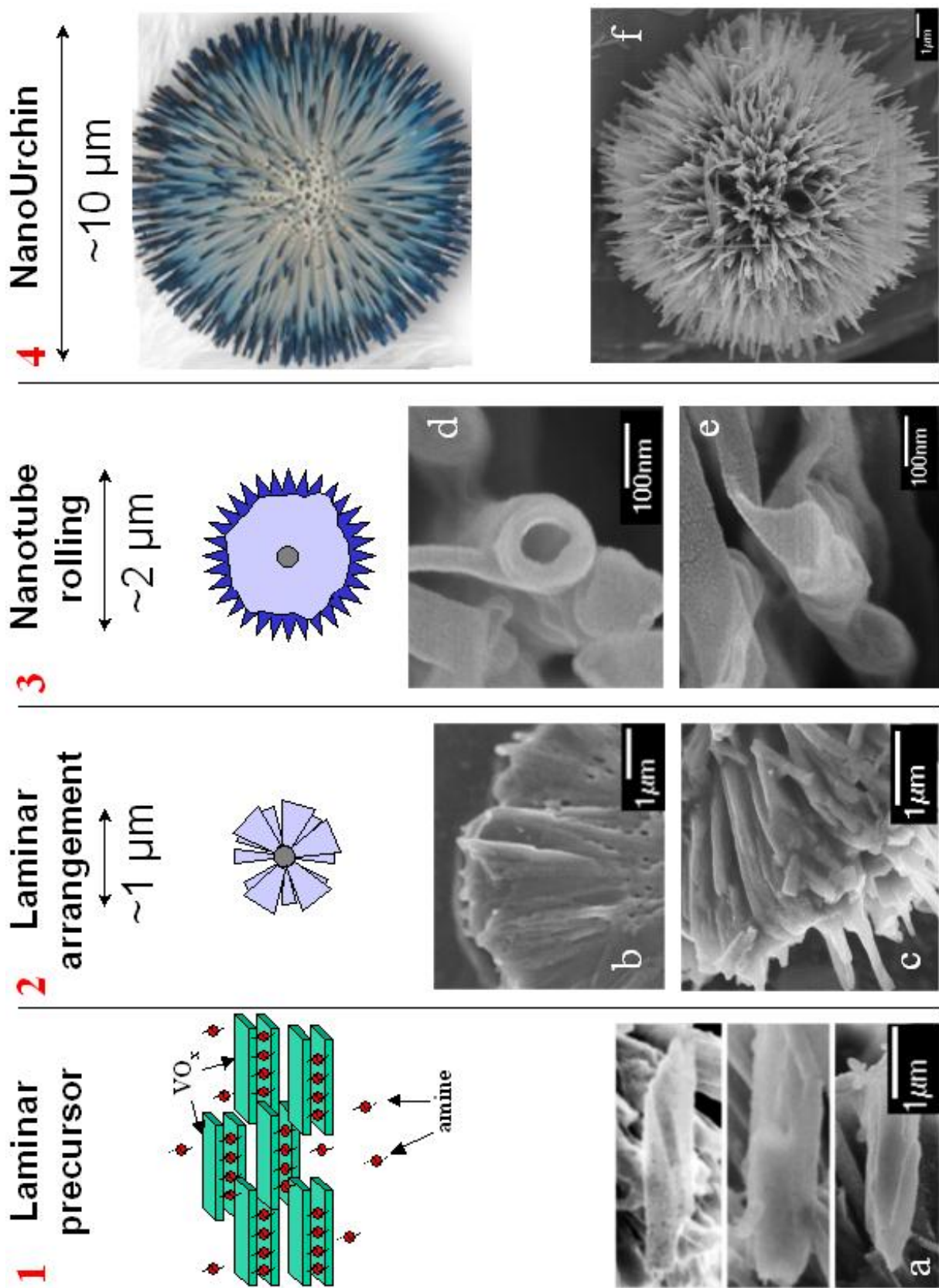


Fig. 13